Hybrid Model Predictive Control for the Stabilization of Wheeled Mobile Robots Subject to Wheel Slippage

Shangming Wei, Kasemsak Uthaichana, *Member, IEEE*, Miloš Žefran, and Raymond DeCarlo

***Abstract*— This paper studies the problem of traction control, i.e., how to stabilize a wheeled mobile robot (WMR) subject to wheel slippage to a desired configuration. The WMR is equipped with a rechargeable battery pack which powers electric drives on each wheel. The drives propel the WMR in one mode of operation or recharge the battery pack (recover energy) in a second mode. These modes of operation are controlled, whereas wheel slippage, e.g., due to ice, is an autonomous mode change. The WMR can be thus modeled as a hybrid system with both controlled and autonomous switches. Model predictive control (MPC) for such systems, although robust, typically results in numerical methods of combinatorial complexity. We show that recently developed embedding techniques can be used to formulate numerical algorithms for the hybrid MPC problem that have the same complexity as MPC for smooth systems. We also discuss the numerical techniques that lead to efficient and robust MPC algorithms in detail. Simulations illustrate the effectiveness of the approach.**

***Index Terms*— Embedding, mobile robots, model predictive control, optimal control, switched systems.**

I. Introduction

In THIS paper, we use the techniques developed in [1] and [2] to generate robust traction controls that stabilize wheeled mobile robots (WMRs) subject to wheel slippage to a predefined configuration. Each WMR is equipped with a rechargeable battery pack which powers electric drives on each wheel. The drives propel the WMR in one mode of operation or recharge the battery pack (recover energy) in a second mode. These modes of operation are controlled. Additional modes of operation occur due to switches from rolling to sliding of the wheel caused, for example, by ice. In contrast to the switches in the operation of the electric drives, these switches are autonomous, and thus the WMRs can be modeled as hybrid systems with both controlled switches (a separate input directly controls the mode changes) and autonomous switches (state/input value dependent switches). From [3], the model can be viewed as an abstraction of a four-wheel steered vehicle, and since we presume a rechargeable battery pack, it has properties similar to those of a hybrid electric vehicle [4], [5].

In a general sense, the control systems studied herein exhibit autonomous (uncontrolled) switches and controlled switches, both resulting in discontinuous jumps in the vector fields governing the evolution of the continuous state of the system. However, the autonomous switches undergo discontinuous jumps in the vector fields as a result of the state and the input entering different regions in the combined state and input space. An example of a system with autonomous switches is that of a system subject to continuous state-dependent constraints, i.e., the switches correspond to different combinations of constraints that are active in a particular region of the state space. In the case of controlled switches, the continuous system is assumed to have a finite number of different vector fields, and a controller can switch between them without restrictions. Typically, the controller is determined at a supervisory level. We assume that the set of different operating regimes of the system defined through the autonomous and controlled switches is finite.

The control development uses an extension of the embedding technique in [2] to four modes of operation (two modes for each wheel) to solve a hybrid optimal control problem in the context of a receding horizon model predictive control (HMPC) strategy. An integral quadratic performance index (PI) is set forth to encode the control objectives. The distinguishing features of the proposed methodology are that it reduces to well-understood continuous optimal control approaches and that no assumptions are made on mode sequence or switching instants. The numerical solution utilizes collocation combined with a penalty function methodology implemented as a discrete-time continuation method [6], [7]. Simulation results demonstrate that the approach can effectively solve the traction control problem for the WMRs and show features that are remarkably similar to strategies recommended by driver's manuals (see [33, p. 86]).

Modeling and control of WMRs have been extensively studied in [8]–[12], among many others. Much of the work assumes that contact between the wheels and the ground satisfies the conditions of pure rolling, avoiding the problems associated with slipping or sliding. For example, [13] uses

Manuscript received July 12, 2011; revised June 20, 2012; accepted September 25, 2012. Manuscript received in final form November 8, 2012. Date of publication August 15, 2013; date of current version October 15, 2013. Recommended by Associate Editor R. Landers.

S. Wei is with MathWorks, Natick, MA 01760 USA (e-mail: shangmingwei@gmail.com).

K. Uthaichana is with the Electrical Engineering Department, Chiang Mai University, Chiang Mai 50200, Thailand (e-mail: kasemsak@chiangmai.ac.th).

M. Žefran is with the Department of Electrical and Computer Engineering, University of Illinois at Chicago, Chicago, IL 60604 USA (e-mail: mzefran@uic.edu).

R. DeCarlo is with the School of Electrical and Computer Engineering, Purdue University, West Lafayette, IN 47907-2017 USA (e-mail: decarlo@ecn.purdue.edu).

Color versions of one or more of the figures in this paper are available online at http://ieeexplore.ieee.org.

Digital Object Identifier 10.1109/TCST.2012.2227964

MPC for tracking control of a nonholonomic WMR, under the condition of only pure rolling. Wheel slippage can easily occur when a WMR moves on a slippery surface, when it makes a high speed turn, or when the torques applied to the wheels are sufficiently large. The WMRs dynamics change when the wheels switch between rolling and sliding. During sliding, controllability fails, making stabilization to a predefined set [14] problematic.

Although some studies (e.g., [15], [16]) have considered the skidding and slipping effects, the proposed controllers are neither closed-loop nor robust. Consequently, adequate performance cannot be guaranteed in the presence of uncertain parameters, unmodeled friction, and external disturbances. In [17], the authors model a Hilare-type WMR with rolling and sliding as a hybrid system and develop a stabilizing switching controller. This paper develops an alternative hybrid (traction) controller that more easily generalizes to a larger class of systems while providing robust performance even during sliding.

Based on the result in [1] and [2], we show that, for quite a general class of hybrid (switched) optimal control problems, the computational complexity of the problem is no greater than that of smooth optimal control problems. We show that the approach from [1] and [2] can be readily applied to systems with an arbitrary number of modes and that autonomous modes are easily incorporated into the embedding framework.

This paper is organized as follows. Section II describes the dynamics of the Hilare robot and the various modes of operation. Section III provides an overview of the embedding approach to switched optimal control. In particular, it points out that, in almost all cases, solutions to the embedded optimal control problem are solutions to the switched optimal control. The specific case where this may not be true requires a terminal set that is closed; thus, it is not possible with model and penalty function used in this paper. In Section IV, the switched control problem to be solved is set forth and the numerical solution methodology discussed, which via the embedding method avoids the use of integer variables. Section V contains the simulation results and discussion. In conclusion, Section VI summarizes the approach and discusses the implications of the results.

II. Hilare Robot Model

A. Dynamic Equations

As in [17], we consider a Hilare robot—a mobile robot with two independently driven wheels—on a horizontal plane (Fig. 1). The wheels of the WMR can either roll or slide (autonomous switches), and a regenerative brake can be turned on or off as necessary (controlled switches). The control torque inputs $u = [\,u_1\ u_2\,]$ drive wheels 1 and 2 with power provided by a rechargeable battery pack. Regenerative braking reduces the amplitude of each wheel's angular velocity (w_1 and w_2) while recharging the battery pack.

The generalized coordinates of the WMR are its center of mass position x and y, body orientation relative to the x-axis θ, and the rotations of the wheels ϕ_1 and ϕ_2. Since we are only interested in controlling position and orientation

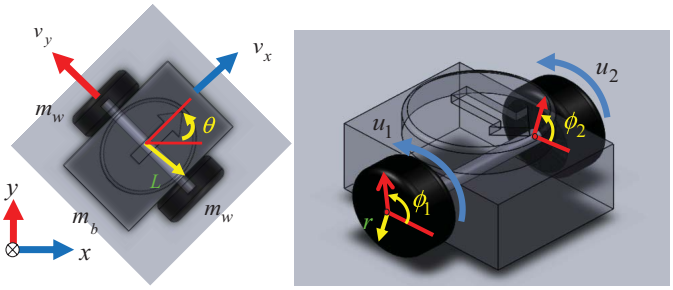

Fig. 1. Top and isometric view of the WMR.

of the robot body, the wheel angles ϕ_1 and ϕ_2 are not relevant; the state variables for the system are thus $z^T = [x, y, \theta, v_x, v_y, \omega, w_1, w_2]^T \in R^8$, where $[v_x, v_y]$ are the velocities of the center of mass of the WMR, expressed in the body frame; $\omega = \dot{\theta}$ is the turning velocity of the WMR; and $w_1 = \dot{\phi}_1$ and $w_2 = \dot{\phi}_2$ are the rotational velocities of the wheels 1 and 2, respectively. The equations of motion for the WMR are

$$\begin{aligned}
\dot{x} &= v_x \cos\theta - v_y \sin\theta, \qquad \dot{v}_x = \omega v_y + \frac{F_x^1 + F_x^2}{m_b + 2m_w} \\
\dot{y} &= v_x \sin\theta + v_y \cos\theta, \qquad \dot{v}_y = -\omega v_x + \frac{F_y^1 + F_y^2}{m_b + 2m_w} \\
\dot{\theta} &= \omega, \qquad \dot{\omega} = L\frac{F_x^1 - F_x^2}{I_b + 2I_v} \\
\dot{w}_1 &= \frac{F_x^1 r + u_1}{I_w}, \qquad \dot{w}_2 = \frac{F_x^2 r + u_2}{I_w}
\end{aligned} \tag{1}$$

where m_b is the mass of the WMRs body; m_w is the mass of a wheel; I_b and I_v are the moments of inertia of the WMR's body, and a wheel, respectively, about a vertical axis through the center of mass; I_w is the moment of inertia of a wheel around its rotational axis; and L and r are the half-width of the robot body and radius of the wheel, respectively. All these parameters are known. Finally, F_x^i and F_y^i are the forces between the ground and the ith wheel in the forward and the lateral direction, respectively, expressed in the body frame. They correspond to frictional forces when a wheel is sliding and constraint forces if the wheel is rolling.

When the ith wheel is rolling, the relative velocity between the ground and the point of contact of the ith wheel is zero

$$v_r^i = \begin{bmatrix} v_{rx}^i \\ v_{ry}^i \end{bmatrix} = \begin{bmatrix} v_x \pm L\omega + r w_i \\ v_y \end{bmatrix} = \begin{bmatrix} 0 \\ 0 \end{bmatrix} \tag{2}$$

where the "+" sign applies to wheel 1 and the "−" sign to wheel 2. Also, during rolling, F_x^i and F_y^i are ground reaction forces that prevent wheel slippage; they can be eliminated from (1) using the rolling constraints (2) [35]. An autonomous switch from rolling to sliding occurs when the magnitude of the constraint force $F^i = [\,F_x^i\ F_y^i\,]^T$ exceeds the maximum possible magnitude of the static friction

$$\left\| F^i \right\| > \mu_s \left(\frac{m_b}{2} + m_w \right) g \quad \Rightarrow \quad \text{rolling} \rightarrow \text{sliding} \tag{3}$$

where μ_s is the (known) coefficient of static friction at the point of contact between the wheel and the ground.

When wheel i is sliding, F_x^i and F_y^i are frictional forces arising from Coulomb's law[1]

$$\begin{bmatrix} F_x^i \\ F_y^i \end{bmatrix} = -\mu_d \frac{\left(\frac{m_b}{2} + m_\omega\right) g}{\left\| v_r^i \right\|} \begin{bmatrix} v_{rx}^i \\ v_{ry}^i \end{bmatrix}. \tag{4}$$

In (4), μ_d is the (known) coefficient of dynamic friction at the point of contact between the wheel and the ground. In this case, the switch from sliding to rolling occurs when: 1) $v_r^i = [v_{rx}^i, v_{ry}^i]^T = 0$, and 2) the maximum magnitude of the frictional force exceeds that of the constraint force F^i

$$\begin{aligned} v_r^i \;&=\; 0 \text{ and } \left\| F^i \right\| \le \mu_s \left(\frac{m_b}{2} + m_w\right) g \\ &\Rightarrow \text{ sliding} \rightarrow \text{rolling.} \end{aligned} \tag{5}$$

We assume that $\mu_d < \mu_s$, which is consistent with the physics of friction.

In addition to the autonomous switches, where the system switches between rolling and sliding depending on the physics of the contact, the system also has controlled switches (mode switches) where the regenerative brake can be switched on or off arbitrarily. Physically, engaging a regenerative brake requires changing the mode of operation of the electric motor driving the wheel from propelling to braking. In other words, controlled switches correspond to changing the electric signals that control the electric motor circuitry. When the regenerative brake is off, the actuating torques of both wheels are constrained as follows:

$$u_i = u_i^1 \triangleq F_1^i \in [-30, 30], \qquad i = 1, 2. \tag{6}$$

However, when the regenerative brake is on

$$u_i = u_i^2 \triangleq F_2^i = \begin{cases} -K_b w_i, & |w_i| \le 3 \\ -30 sgn(w_i), & |w_i| > 3 \end{cases} \quad i = 1, 2 \tag{7}$$

where $K_b = 10$ is a fixed regenerative braking coefficient. Note that u_i saturates at 30 Nm regardless of whether the regenerative brake is on or off.

Equation (1) constitutes the state model with state and control constraints determined by (2)–(7). Because of the switches between rolling and sliding, and because an electric drive can change its mode of operation between braking and propelling, the above model represents a switched system.The autonomous switches (switches between rolling and sliding) result when the state/control-torque trajectories $(z(t), u(t))$ cross the fixed hypersurfaces described by (2)–(5) in the state/control-torque space. A switch from rolling to sliding can be induced by changing the wheel torque, but once the wheel is sliding, no control can instantaneously bring it to rolling. Instead, controlled switches (the change in the mode of operation of the electric drive) can occur at an arbitrary point (z, u). In the rest of this paper, we will associate *mode* with controlled switches, and *regime* with autonomous switches. The system above thus has four modes of operation (which can be chosen by controlled switches), two modes for wheel 1, and two modes for wheel 2. Modes will be labeled as *pp* (mode 1) when wheels 1 and 2 are propelling, *pb* (mode 2) when wheel 1 is propelling and wheel 2 is braking, *bp* (mode 3) when wheel 1 is braking and wheel 2 is propelling, and *bb* (mode 4) when both wheels are braking. The system also has four regimes that will be labeled *rr* when both wheels are rolling, *sr* when wheel 1 is sliding and wheel 2 is rolling, *rs* when wheel 1 is rolling and wheel 2 is sliding, and *ss* when both wheels are sliding.

Table I summarizes both modes and regimes for the Hilare robot with regenerative braking. As described in Section III-A, different regimes (and thus the autonomous switches) can be taken into account by allowing the vector fields associated with each mode to be piecewise continuous (see below).

[1]More complicated friction models for stick–slip transition such as Dahl's model and Lugre's model are available but are beyond the scope of this paper.

B. Well-Posedness of the Model

The behavior of a switched system with autonomous switches can be quite complex and might exhibit Zeno behavior or deadlock states. In general, it is thus necessary to establish existence and uniqueness of solutions to the system equations.

For the Hilare robot described above, the existence and uniqueness of solutions can be shown directly. We only focus on autonomous switches since by design only a finite number of controlled switches occurs on any finite time interval. Furthermore, when a wheel is rolling, constraints (2) imply that the system state z evolves on a lower dimensional manifold where the relative velocity between the wheel and the ground equals 0. If a switch from rolling to sliding occurs, the relative velocity becomes nonzero since static friction is strictly greater than dynamic friction. According to (5), a switch back from sliding to rolling thus cannot occur in zero time; indeed, the relative velocity can only be reduced back to 0 over a nonzero time interval. Thus, the existence and uniqueness of solutions for the Hilare robot is guaranteed.

III. Theoretical Foundations

A. Switched Systems With Autonomous Switches

In this section we review the methodology presented in [1] and [2], which builds on the earlier work of [18]. Motivated by the treatment of the autonomous switches in [19] and [37], and by features of the Hilare robot model in Section II, we consider systems of the form

$$\dot{z}(t) = \sum_{k=1}^{d_\alpha} \alpha_k(t) f_k\left(z(t), u(t)\right), \qquad z(t_0) = z_0 \tag{8}$$

such that

$$\sum_{k=1}^{d_\alpha} \alpha_k(t) = 1 \tag{9}$$

where $z(t) \in \mathrm{R}^n$ is the continuous state; $u(t) \in \mathrm{R}^m$ is the continuous control input that is assumed to be a measurable function; $\alpha_k \in \{0, 1\}, k \in D_\alpha = \{1, \ldots, d_\alpha\}$ is a measurable function that selects one of d_α possible modes (enabling controlled switches); and $f_k(z, u) : \mathrm{R}^n \times \mathrm{R}^m \rightarrow \mathrm{R}^n$ is a piecewise C^1 vector field defined as follows. We assume that the domain $\mathrm{R}^n \times \mathrm{R}^m$ is partitioned into a finite number d_G of nonempty disjoint smooth submanifolds G_i. Each submanifold

TABLE I
AUTONOMOUS AND CONTROLLED SWITCHES FOR THE HILARE ROBOT WITH REGENERATIVE BRAKING

Autonomous Switches		Controlled Switches	
Regime	**Equation**	**Mode**	**Equation**
rr (wheels 1 and 2 rolling)	$v_r^1 = 0$ $v_r^2 = 0$	*pp* (wheels 1 and 2 propelling)	u_1 given by (6) u_2 given by (6)
sr (wheel 1 rolling, wheel 2 sliding)	$v_r^1 = 0$ $v_r^2 \neq 0$, F^2 as in (4)	*pb* (wheel 1 is propelling, wheel 2 braking)	u_1 given by (6) u_2 given by (7)
rs (wheel 1 sliding, wheel 2 rolling)	$v_r^1 \neq 0$, F^1 as in (4) $v_r^2 = 0$	*bp* (wheel 1 is braking, wheel 2 propelling)	u_1 given by (7) u_2 given by (6)
ss (wheels 1 and 2 sliding)	$v_r^1 \neq 0$, F^1 as in (4) $v_r^2 \neq 0$, F^2 as in (4)	*bb* (wheels 1 and 2 braking)	u_1 given by (7) u_2 given by (7)

G_i has codimension $p_i \geq 0$. When $p_i > 0$, G_i is described by a pair of C^1 functions $\sigma_i : \mathrm{R}^n \to \mathrm{R}^{p_i}$ and $\beta_i : \mathrm{R}^n \times \mathrm{R}^m \to \mathrm{R}^{q_i}$ ($q_i > 0$), where the Jacobian $(\partial \sigma_i / \partial z)$ has full rank everywhere. Let $S_i = \{(z,u) \in \mathrm{R}^n \times \mathrm{R}^m | \sigma_i(z) = 0, \beta_i(z,u) < 0\}$ (the inequalities are taken component-wise), $\partial S_i = \{(z,u) \in \mathrm{R}^n \times \mathrm{R}^m | \sigma_i(z) = 0, \beta_i(z,u) = 0\}$ and $\bar{S}_i = S_i \cup \partial S_i$. We then define $G_i = S_i \backslash M_{p_i}$ where $M_k = \bigcup_{p_i > k} \bar{S}_i$. When $p_i = 0$, the construction of G_i is analogous, except that the function σ_i is absent. In both cases, we define the boundary of G_i to be $\partial G_i = \bar{S}_i \backslash G_i$. For each $k \in D_\alpha$, the vector field $f_k(z,u)$ is C^1 on each submanifold G_i and, if $(z,u) \in G_i$, then $f_k(z,u)$ is tangent to G_i at (z,u). The trajectory $(z(t), u(t))$ can only leave G_i through ∂G_i. Since discontinuities in $f_k(z,u)$ determine the autonomous switches and the boundary points in ∂G_i depend on u, we need to impose conditions that prevent instantaneously reversible switches due to changes in u. Formally, if for some state value $z_0 \in \mathrm{R}^n$ there exists values of the control input u_0 and u_{ij} so that $(z_0, u_0) \in G_i$ and $(z_0, u_{ij}) \in \partial G_i$, and at (z_0, u_{ij}) a switch occurs from G_i to G_j, then it is not possible to switch from G_j to G_i at the point $(z_0, \cdot)$ for any value of control u.

In Section II, the regimes *rr*, *rs*, *sr*, and *ss* can be associated to submanifolds G_{rr}, G_{rs}, G_{sr}, and G_{ss} with codimensions 3, 2, 2, and 0, respectively [the rolling constraint (2) for each wheel results in two equality constraints, but if both wheels are rolling, only three of these equality constraints are independent]. Equation (2) applied to the appropriate wheel defines the functions σ_{rr}, σ_{rs}, and σ_{sr}. The conditions (inequalities) in (3) and (5), which depend both on the state z and the control input u, define the functions β. It is easy to verify that the Jacobian of the functions σ is full rank everywhere. Furthermore, as discussed in Section II-B, instantaneous back-and-forth switches between rolling and sliding are not possible. The model of the Hilare robot thus conforms with (in fact, it motivates) the modeling approach above.

The system in (8) has discontinuous right-hand sides [19], [20] so questions of existence and uniqueness of solutions need to be carefully studied. Systems of differential equations with discontinuous right-hand sides are the subject of [37] and [38], and are rigorously studied in the variable structure control literature as well [34]. Existence of solutions for hybrid automata (without control variables) is studied in [35]. While certainly important, these issues are outside the scope of this paper and we will assume that both existence and uniqueness (in the appropriate sense) are guaranteed.

B. Switched Optimal Control Problem (SOCP)

We are interested in computing optimal control laws for the system described by (8). If there are no controlled switches, $d_\alpha = 1$, i.e., only one mode of operation, only the continuous input $u(t)$ needs to be computed. In this case, the complexity of the optimal control problem reduces to the traditional case. In contrast, for systems with controlled switches we can choose to compute the sequence of switching times $t_1 \ldots, t_{n-1}$ (including n), the sequence of discrete inputs $\alpha_1, \ldots, \alpha_n$, as well as the continuous input $u(t)$ on each interval $[t_j, t_{j+1}]$ for $j = 0, \ldots, n-1$. Therefore it would appear that, for systems with controlled switches, the optimal control problem has combinatorial complexity. In this paper, we show that actually both these cases have the same complexity and are amenable to traditional nonlinear programming techniques such as sequential quadratic programming (SQP) [21], [22]. This further implies that, for the systems with autonomous switches and controlled switches defined in Section III-A, the optimal control problem is no more complex than the traditional smooth problem.

To this end, we now develop the SOCP. Here we require that the continuous control $u(t)$ and the switching control $\alpha_k \in \{0,1\}, k \in D_\alpha$ be chosen on the interval $[t_0, t_f]$ so that any terminal constraints are satisfied and a performance metric is minimized. Specifically, for the boundary conditions, we require that initially $(t_0, z(t_0)) \in T_0 \times B_0$ and at $t = t_f$,$(t_f, z(t_f)) \in T_f \times B_f$; further, we assume that $B = T_0 \times B_0 \times T_f \times B_f \subset \mathrm{R}^{2n+2}$ be compact. The PI, associated with (8), takes the form

$$J_S(t_0, z_0, u, \alpha) = g(t_0, z_0, t_f, z_f) + \int_{t_0}^{t_f} \sum_{k=0}^{d_\alpha} \alpha_k(t) F_k^0(z(t), u(t)) dt \quad (10)$$

where the $\alpha_k(t)$ are subject to (9) and the piecewise C^1 integrands $F_k^0(z,u)$ characterize desired performance in each mode of operation.

The SOCP is thus defined as

$$\min_{u \in \Omega,\ \alpha_k \in \{0,1\},\ k \in D_\alpha} J_S(t_0, z_0, u, \ldots, \alpha_k, \ldots) \quad (11)$$

such that (8) and (9), the boundary conditions, $(t_0, z(t_0)) \in T_0 \times B_0$ and $(t_f, z(t_f)) \in T_f \times B_f$, where the set $\Omega \subseteq \mathrm{R}^m$ is compact and convex, and any other constraints on the controls or state.

C. Embedded Model Formulation and the Embedded SOCP (ESOCP)

The embedded form of the hybrid model of (8) and (9) is obtained by relaxing the condition $\alpha_k \in \{0, 1\}, k \in D_\alpha$ to $\alpha_{Ek} \in [0, 1], k \in D_\alpha$ and by introducing a distinct continuous control input for each mode of operation. We denote the embedded form of the hybrid system as

$$\dot{z}_E(t) = \sum_{k=1}^{d_\alpha} \alpha_{Ek}(t) f_k\left(z_E(t), u_k(t)\right) \tag{12}$$

such that

$$\sum_{k=1}^{d_\alpha} \alpha_{Ek}(t) = 1. \tag{13}$$

For the embedded system (12) and (13), several or all modes may be simultaneously active.

The trajectories of the switched system (8) and (9) are dense in the trajectories of the embedded system (12) and (13), making arbitrarily close approximations of an embedded system trajectory by a switched system trajectory possible. Under the relaxation given above on $\alpha_k(t)$, we have the so-called embedded form of PI

$$\begin{aligned} &J_E(t_0, z_0, \ldots, u_k, \ldots, \alpha_{Ek}, \ldots) \\ &= g(t_0, z_0, t_f, z_E(t_f)) + \int_{t_0}^{t_f} \sum_{k=0}^{d_\alpha} \alpha_{Ek}(t) F_k^0\left(z_E(t), u_k(t)\right) dt. \end{aligned} \tag{14}$$

The embedded system and PI lead naturally to the embedded SOCP, denoted ESOCP, given as

$$\min_{u_k \in \Omega,\ \alpha_{Ek} \in [0,1],\ k \in D_\alpha} J_E(t_0, z_0, t_f, z_E(t_f), u_k, \alpha_{Ek}) \tag{15}$$

subject to (12), (13), the boundary conditions, $(t_0, z_E(t_0)) \in T_0 \times B_0$ and $(t_f, z_E(t_f)) \in T_f \times B_f$, $u_k(t) \in \Omega$ for the compact convex set $\Omega \subseteq \mathrm{R}^m$, and any other constraints on the controls or state; generally we require that any additional constraints on the controls leave the admissible regions convex. The ESOCP is a classical optimization problem and can be solved using existing nonlinear convex programming algorithms; this avoids the search and optimize iterations (combinatorial complexity) associated with mixed-integer programming approaches. Finding bang-bang solutions, when they exist, is generally not problematic because non-bang-bang solutions require that two or more of the largest mode-specific Hamiltonians be equal as described in [2], which is rare. Typically, the numerical algorithm will then naturally converge to a solution which is bang-bang almost everywhere.

D. Existence of Solutions

For the ESOCP defined above, in addition to the assumptions already made (the terminal set is compact and the input constraint Ω is compact and convex), we assume that the set of vector fields are affine in the continuous control variable

$$f_k(z, u_0) = A_k(z) + B_k(z) \cdot u_k$$

and the integrands $F_k^0(z, u_k)$ of the PI are convex in u_k for each (t, z). In sum, these conditions guarantee the existence of a solution to the ESOCP and are satisfied by the Hilare robot model presented in Section II.

E. Relationship Between SOCP and ESOCP

A straightforward extension of Corollary 2 in [2] verifies that the trajectories of the switched system (8) are dense in the trajectory set of the embedded system (12). In addition, [2] extends the chattering lemma to formally show how trajectories of the embedded system can be approximated to an arbitrary precision by trajectories of the switched system. Thus it is possible and reasonable to generate optimal solutions for the SOCP by solving the ESOCP, a classical (convex) optimization problem, with a possibly nonunique solution existing under the conditions cited above. Further, the ESOCP is not subject to combinatorial complexity. Hence, an optimal solution of the ESOCP, $(z_E^*, u_k^*, \alpha_{Ek}^*)$[2] can either be a solution to the SOCP or be approximated with arbitrary precision by a trajectory of the switched system. Note that, under the conditions cited above, the ESOCP always has a solution whereas the SOCP may not. However, according to [2], if the SOCP does not have a solution

$$\begin{aligned} &\min_{u_k \in \Omega,\ \alpha_{Ek} \in [0,1],\ k \in D_\alpha} J_E(t_0, z_0, t_f, z_E(t_f), u_k, \alpha_{Ek}) \\ &\quad = \inf_{u \in \Omega,\ \alpha_k \in \{0,1\},\ k \in D_\alpha} J_S(t_0, z_0, t_f, z(t_f), u, \alpha_k). \end{aligned} \tag{16}$$

While [2] provides a constructive method of approximating an embedded trajectory with a switched trajectory, the method is complex and numerically cumbersome. Hence, it is desirable to develop heuristic methods that are more easily implemented. Some work in this open research direction is described in [31]. In this paper (see also [32]), we use a duty cycle interpretation of α_{Ek}, which proved sufficient.

There are four additional points regarding the relationship of the ESOCP and SOCP: 1) even when the sufficient conditions for the existence of an ESOCP solution are met, the SOCP is not guaranteed to have a solution, in which case (16) holds; 2) the optimal value of J_E always lower bounds the value of J_S for the SOCP, since the optimization is over a wider function class that includes all those pertinent to the SOCP; and 3) when the ESOCP has a bang-bang optimal solution, i.e., there exists a set of $\alpha_{Ek}^* \in \{0, 1\},\ k \in D_\alpha$, it also optimally solves the SOCP. The main relationships are summarized in Table II.

As seen in Table II, the presence of singular solutions, with $\alpha_{Ek}^* \in \{0, 1\}, k \in D_\alpha$, can reveal situations when

[2]We are using the shorthand notation $(z_E^*, u_k^*, \alpha_{Ek}^*)$ to mean $(z_E^*, u_1^*, \ldots, u_{d_\alpha}^*, \alpha_{E1}^*, \ldots, \alpha_{Ed_\alpha}^*)$.

the SOCP does not have solutions. Singular solutions are those for which two or more of the largest mode-specific Hamiltonians (see [2]) are equal. In the case of a two-switched system, for which $\alpha(t)$ and $(1-\alpha(t))$ represent the two modes of operation, the Hamiltonian has the structure $\alpha(t)\cdot E_1(t,z,u_0,u_1,\lambda^0,\lambda) + E_2(t,z,u_0,u_1,\lambda^0,\lambda)$. If the function $E_1(t,z,u_0,u_1,\lambda^0,\lambda)\equiv 0$ over some time interval(s) of nonzero measure, then $\alpha(t)$ would appear to be arbitrary over those intervals. In such cases, maximizing the Hamiltonian does not identify the optimal switching function. Other boundary, physical or higher order optimality conditions may restrict the choices of the α_{Ek}^*'s as there may be an infinite number of solutions.

The only case, isolated SOCP solution, when the ESOCP may not necessarily solve the SOCP, is when: 1) the ESOCP has no bang-bang solution; and 2) the end-state of the embedded system trajectory $z_E^*(t_f)$ lies on the boundary of the closed set B_f. In this case, the end-states of approximating switched trajectories to an ESOCP solution are not guaranteed to meet the final constraint. This case has not been completely studied, and the current analysis does not exclude its existence. In many engineering applications, the terminal set of the SOCP can be approximated with an open set. Hence, approximate solutions of the SOCP can always be constructed, motivating a continued focus on the embedding approach.

IV. PI and Solution Methodology

A. Embedded Model of the WMR

Using the development described in Section III, we can express the WMR embedded model as

$$\dot{z} = \sum_{k\in D_{\mathrm{WMR}}} \alpha_{Ek} f_k(z,u_k) \tag{17}$$

where $D_{\mathrm{WMR}} = \{pp, pb, bp, bb\}$.

Let us further denote the constraints by the general function

$$h(z,u_k,\alpha_{Ek}) \le 0. \tag{18}$$

Our goal is to solve an ESOCP

$$\min_{u_k\in\Omega,\alpha_{Ek}\in[0,1],k\in D_{\mathrm{WMR}}} J_E(t_0,z_0,u_k,\alpha_{Ek}) \tag{19}$$

subject to (17) and (18), for a specific J_E as developed in the next section.

B. Control Objective Overview

The objective of the control design is to drive the WMR from a given initial state $z_0^T = [x(0), y(0), \theta(0), v_x(0), v_y(0), \omega(0), w_1(0), w_2(0)]^T$ to a predefined set/state $z_f^T = [x(T), y(T), \theta(T), v_x(T), v_y(T), \omega(T), w_1(T), w_2(T)]^T$, within an allotted time T, while minimizing a performance index that includes energy usage. Note that $z_f \in B_f$ may have free entries. For example, if the task is to command the WMR to drive along the line $y=1$ with a constant forward velocity v_0, then $z_f^T = [x(T), 1, 0, v_0, 0, 0, -(v_0/r), -(v_0/r)]^T$ and there is no requirement for $x(T)$. In addition to minimizing energy usage while achieving the objective, we also desire to minimize the (undesirable) sliding of the wheels as it implies the loss of controllability. This leads us to consider the nominal cost functional

$$J_E^{\mathrm{nom}} = \int_0^T \Big[c_1\left(\alpha_{Epp}+\alpha_{Epb}\right)u_1^2 + c_2\left(\alpha_{Epp}+\alpha_{Ebp}\right)u_2^2 + c_3\left\|v_r\right\|^2 \Big] dt. \tag{20}$$

The term $c_1(\alpha_{Epp}+\alpha_{Epb})u_1^2$ penalizes the actuating power usage of wheel 1; $c_2(\alpha_{Epp}+\alpha_{Ebp})u_2^2$ penalizes the actuating power usage of wheel 2; and $c_3\|v_r\|^2$ penalizes and thus limits the sliding motion. There is no penalty for regenerative braking usage.

There are two problems associated with numerically solving this optimization problem. First, because the system is stabilizable but not controllable when sliding, using hard constraints could make the optimal control problem infeasible. We thus enforce the boundary conditions as soft constraints, resulting in the cost functional

$$J_E^{\mathrm{bnd}} = c_0\left\|z(T)-Z_f\right\|^2 + J_E^{\mathrm{nom}}. \tag{21}$$

The term $c_0\|z(T)-z_f\|^2$ drives the final states of the WMR, $z(T)$, toward the desired set. Note that, if the desired final set includes free state variables, they need to be excluded from this term.

The second difficulty is that, when the system's state equations are imposed as hard constraints, the solution becomes numerically difficult to compute. We therefore use the quadratic penalty function method [22] to numerically solve the optimization problem.

C. Quadratic Penalty Function Method

In quadratic penalty function method, a solution of the constrained optimization problem is obtained by solving a sequence of unconstrained problems. Consider the optimization

$$\min_{z\in Z} F^0(z) \quad \text{such that } h(z)=0 \tag{22}$$

where $F^0: R^n \to R$ and $h: R^n \to R^m$ are given functions with $Z\subset R^n$ a given subset. For any scalar $c>0$, define the augmented Lagrangian $L_c: R^n\times R^m \to R$ by

$$L_c(z) = F^0(z) + \frac{1}{2}c\left|h(z)\right|^2 \tag{23}$$

where c is a penalty parameter. Instead of solving the original problem (22), we would like to solve a sequence of problems of the form

$$\min_{z\in Z} L_{c_n}(z) \tag{24}$$

where $\{c_n\}$ denotes a penalty parameter sequence satisfying

$$0 < c_n < c_{n+1} \quad \forall n,\ c_n \to \infty. \tag{25}$$

If we can construct a sequence of approximate problems that converges in a well-defined sense to the original problem, then the corresponding sequence of the approximate solutions will yield in the limit a solution of the original problem, as

TABLE II
RELATIONSHIP BETWEEN SOCP AND ESOCP SOLUTIONS

ESOCP Sols	SOCP Sols	Remarks
Bang-bang solutions exist: there exists $\alpha^*_{Ek} \in \{0,1\}, k \in D_\alpha$	At least one ESOCP Solution is a SOCP Solution	SOCP solved
All ESOCP solutions are non-bang: largest of two or more of mode-specific Hamiltonians are equal, implying $\exists k \in D_\alpha$ such that $\alpha^*_{Ek} \in (0,1)$ over some nonzero time interval(s)	Isolated bang-bang SOCP Solution: $z^*(t_f) \notin Int(B_f)$	ESOCP does not solve SOCP. ESOCP has lower cost PI. Approximate ESOCP solution with a switched trajectory
	No SOCP solution. $z^*(t_f) \in Int(B_f)$	Approximate ESOCP solution with a switched trajectory.

is shown in [23]. The literature often terms such approaches continuation methods [6], [7].

In the context of the quadratic penalty function method, the PI for the WMR will take the form

$$J_{En} = J_E^{\text{bnd}} + \int_0^T c_{4n} \left\| \text{DE}_1 - \text{DE}_2 \right\|^2 dt \tag{26}$$

where DE_1 and DE_2 are the left-hand sides and the right-hand sides of (17) derived from (1), and the term $c_{4n}\|\text{DE}_1 - \text{DE}_2\|^2$ progressively enforces the state equation constraints. In this context, the resulting ESOCP is

$$\min_{u_k \in \Omega, \alpha_{Ek} \in [0,1], k \in D_{\text{WMR}}} J_E = \lim_{n \to \infty} \min_{u_k \in \Omega, \alpha_{Ek} \in [0,1], k \in D_{\text{WMR}}} J_{En}. \tag{27}$$

D. MPC Design

To cope with disturbances and modeling uncertainties, an MPC-type controller [24] with a receding finite horizon window is utilized. This type of MPC can be summarized as follows.

1) Given z_0, partition the finite horizon window of time length T into N equal subintervals of length $\Delta t = (T/N) \stackrel{\Delta}{=} h$ to compute a (backward) piecewise constant control sequence $\{\widehat{u}_1, \ldots, \widehat{u}_N\}$ where $\widehat{u}_j^T = [u_1((j-1)h) \quad u_2((j-1)h)]$ and the associated state vectors $\{z_1, \ldots, z_N\}$. Define $t_j = t_0 + j\frac{T}{N}, j = 1, \ldots, N$.
2) Solve the optimization of (27) for the continuous controls $\{\widehat{u}_1, \ldots, \widehat{u}_N\}$ and the switching controls $\{\alpha_E^1, \ldots, \alpha_E^N\}$ where $\alpha_E^j = [\alpha_{Epp}^j, \alpha_{Epb}^j, \alpha_{Ebp}^j, \alpha_{Ebb}^j]^T$.
3) Apply the control $\widehat{u}_1$ and the (appropriately approximated, see Section III-E) switching control α_E^1 to the system over the time interval $[t_0, t_1]$ and measure the state $z(t_1)$.
4) Decrement the horizon window by 1 to form a new time window over $[t_j, t_N]$, with measured initial condition $z(t_j)$. Repeat steps 2 and 3 until $j = N$, applying the computed controls $\widehat{u}_j$ and α_E^j to the model over the time interval $t_{j-1} \le t < t_j$.

Other MPC strategies exist, for example, in which the horizon window is of a fixed length until it intercepts the final time after which it shrinks until the optimization is completed. We note at this point that our solution methodology is conceptually quite distinct from existing hybrid MPC approaches such as [25], which employ mixed-integer programming. With the embedding approach proposed herein, there is no need for computationally expensive combinatorial search over possible mode sequences.

E. Numerical Method

Given the embedded PI and the state equation and constraints of Sections III and IV, one discretizes these equations using the collocation method. These discretized equations convert the ESOCP into a finite-dimensional nonlinear programming problem (NLP) where states and inputs are treated as unknown variables. The NLP can be solved using an SQP solver, such as fmincon in the optimization toolbox of MATLAB. The discretization-and-collocation technique consists of several steps that have two main stages: 1) time discretization, and state and input function approximations by a finite number of polynomial basis functions; and 2) approximation of the continuous state dynamics and the performance integrand by discrete-state and discrete-input-dependent counterparts.

Without going through a lengthy derivation, the continuous time interval $[t_0, t_f]$ is discretized into a sequence of points $t_0 < t_1 < t_2 < \cdots < t_{N-1} < t_N = T$ where, for simplicity, we adopt an equi-length time interval $t_j - t_{j-1} = h$, for $j = 1, \ldots, N$. A hat notation is also used to distinguish the numerically estimated state and control values from their actual counterparts that are hatless, e.g., $\hat{z}_j = \hat{z}(t_j)$, $\hat{u}_{kj} = \hat{u}_k(t_j)$, and $\hat{\alpha}_E^j = \hat{\alpha}_E(t_j)$. The collocation method used here assumes triangular basis functions for the state and piecewise constant basis functions (derivatives of triangular functions) for the controls. Specifically, the estimated state is given by

$$\hat{z}(t) = \sum_{j=0}^{N} \hat{z}_j \phi_j(t) \tag{28}$$

where the $\hat{z}_j$ are to be determined and the triangular basis functions are given by

$$\phi_j(t) = \begin{cases} \frac{t - t_{j-1}}{\Delta t}, & t_{j-1} < t \le t_j \\ \frac{t_{j+1} - t}{\Delta t} & t_j < t \le t_{j+1} \\ 0, & \text{elsewhere.} \end{cases} \tag{29}$$

Note that the method is not restricted to using triangular basis functions, and that each of the $\phi_j(t)$s is a time shift of the previous one.

As summarized in [26], the theoretical approach for computing the controls is to extend the state space with new state variables $z_{ext} \in R^{m+d_\alpha}$ whose derivatives are the desired controls $u(t) \in R^m$ and $\alpha_{Ek}(t) \in [0,\ 1] \subset R$, for $\forall\, k \in D_\alpha$, to be computed. However, our choice of triangular basis functions for the states renders the control inputs piecewise constant, and we simply solve directly for these (constant) control values. Specifically, the estimates of the control inputs are given by

$$\begin{bmatrix} \hat{u}_k(t) \\ \hat{\alpha}_E(t) \end{bmatrix} = \sum_{j=1}^{N} \begin{bmatrix} \hat{u}_{kj} \\ \hat{\alpha}_E^j \end{bmatrix} \psi_j(t) \tag{30}$$

where the piecewise constant basis functions are given by

$$\psi_j(t) = \begin{cases} 1, & t_{j-1} < t \le t_j \\ 0, & \text{elsewhere.} \end{cases} \tag{31}$$

Here we note that, by the definition of the basis functions in equation (29), the control values computed at t_j are enforced over the interval $t_{j-1} < t \le t_j$.

The essence of the midpoint rule in the collocation method is to enforce the constraints at the midpoints of each interval $[t_{j-1}, t_j]$ for $j = 1, \ldots, N$. There results the discretized embedded state dynamics

$$\hat{z}_j = \hat{z}_{j-1} + \Delta t \sum_{k=1}^{d_\alpha} \hat{\alpha}_{Ek}^j f_k \left(\frac{\hat{z}_{j-1} + \hat{z}_j}{2}, \hat{u}_{kj} \right) \tag{32}$$

for $j = 1, \ldots, N$, with $f_k(\cdot)$ denoting the discretized state dynamics in each mode, respectively. Thus the solution to the ESOCP is given by the following NLP:

$$\min_{(\hat{u}_{kj}, \hat{\alpha}_{kj}) \in \Omega \times [0,1],\ k \in D_\alpha} \hat{J} \tag{33a}$$

where $\hat{J}$ is the properly discretized performance index (10):

$$\hat{J} = g\left(t_0, \hat{z}_0, t_N, \hat{z}_N\right) + \Delta t \sum_{j=1}^{N} \sum_{k=1}^{d_\alpha} \hat{\alpha}_{Ek}^j \frac{1}{2} \times \left\{ F_k^0\left(t_j, \hat{z}_j, \hat{u}_{kj}\right) + F_k^0\left(t_{j-1}, \hat{z}_{j-1}, \hat{u}_{kj}\right) \right\} \tag{33b}$$

subject to

1) equation (32), i.e.

$$\hat{z}_j = \hat{z}_{j-1} + \Delta t \sum_{k=1}^{d_\alpha} \hat{\alpha}_{Ek}^j f_k \left(\frac{\hat{z}_{j-1} + \hat{z}_j}{2}, \hat{u}_{kj} \right) \tag{33c}$$

2) all other equality constraints represented as $h(\hat{z}_{j-1}, \hat{z}_j, \hat{u}_{kj}, \hat{\alpha}_E^j) = 0$.

V. Simulations

We demonstrate the effectiveness of the proposed methodology through simulations. Each experiment took between 15 and 45 minutes in total, i.e., inclusive of optimization and simulation using the computed controls. We consider the task of driving the WMR to the origin, requiring the robot to reach the origin at a given time. The parameters used in simulations were $m_b = 1$, $m_w = 0.5$, $L = 1$, $r = 4$, $\mu_d = 0.6$, $\mu_s = 0.7$, and $g = 9.8$. In simulations, the WMR is driven from the initial state $z_0^T = [x_0, y_0, \theta_0, v_{x,0}, v_{y,0}, \omega_0, w_{1,0}, w_{2,0}]^T = [0, 4, 1, 1, 2, 0, 0.5, 1]^T$ to the origin, $z_f = 0$, within $T = 8$s. The weights for the cost functional were chosen to be $c_0 = c_3 = 10^3$ and $c_1 = c_2 = 1$. For the quadratic penalty function, the penalty parameter was chosen to be $c_{4k} = 10^k$ for $k = 0, 1, 2, 3, 4$. The number of grid points for this simulation is $N = 80$. Within the MPC context, the first horizon window is 8s with 80 partitions. The first control for $0 \le t < 0.1$s is applied. This is followed by a Runge–Kutta simulation of the physical system that returns the actual state of the physical system $z(0.1)$. The MPC window is then shortened to 7.9s with 79 partitions, and the process is repeated.

We first consider the nominal case when no disturbances are present and the robot has perfect estimates of the static and dynamic coefficients of friction. We shall refer to this simulation as case 1.

Initially, the WMR is rotated by 1rad with respect to the horizontal axis and it is sliding sideways with velocity 1m/s and forward at 2m/s. One notes also that the wheels are spinning. Fig. 2 shows the trajectory, velocities of both wheels, the four controlled modes (regenerative braking is on or off for each wheel), the autonomous modes (each wheel sliding or rolling), and the continuous control inputs (torques) for each wheel. The figures show that both wheels slide initially and are both driven to rolling mode after about 0.4s. Subsequently, active propelling is used to turn the WMR to the left. At about 3.5s, wheel 2 starts regenerative braking, causing the robot to start turning right. The wheel switches to propelling action at 5.4s to achieve further steering action. At about the same time, wheel 1 starts regenerative braking in order to slow the WMR down and reach the origin at $T = 8$s. Note that regenerative braking is coordinated with propelling action both in order to steer the WMR and to control its forward velocity. The WMR reaches the origin successfully at $T = 8$s with zero velocity, achieved by using a short burst of propelling action at both wheels.

There is a short singular solution at around 7.2s for wheel 2 (see discussion of singular solutions in Section III). As discussed in Section III-E, this singular solution can be realized by using the value of $\alpha \in (0, 1)$ as a duty cycle and switching between the brake on/off modes accordingly.

A. Robustness

This subsection looks at the robustness properties of the hybrid MPC (HMPC) scheme. In this effort, a slippery patch is added to the environment. Two different cases are considered. In case 2, the patch is an annulus, $2 \le r \le 2.5$ around the origin in which the static coefficient of friction μ_s drops from 0.7 to 0.002, and the dynamic coefficient of friction μ_d drops from 0.6 to 0.0001. For this case, the robot does not know about the existence of the slippery patch. In contrast, in case 3 the patch is a larger annulus, $1.5 \le r \le 2.5$, around the origin with the same static and dynamic coefficients of friction as above. The robot learns about the slippery patch when

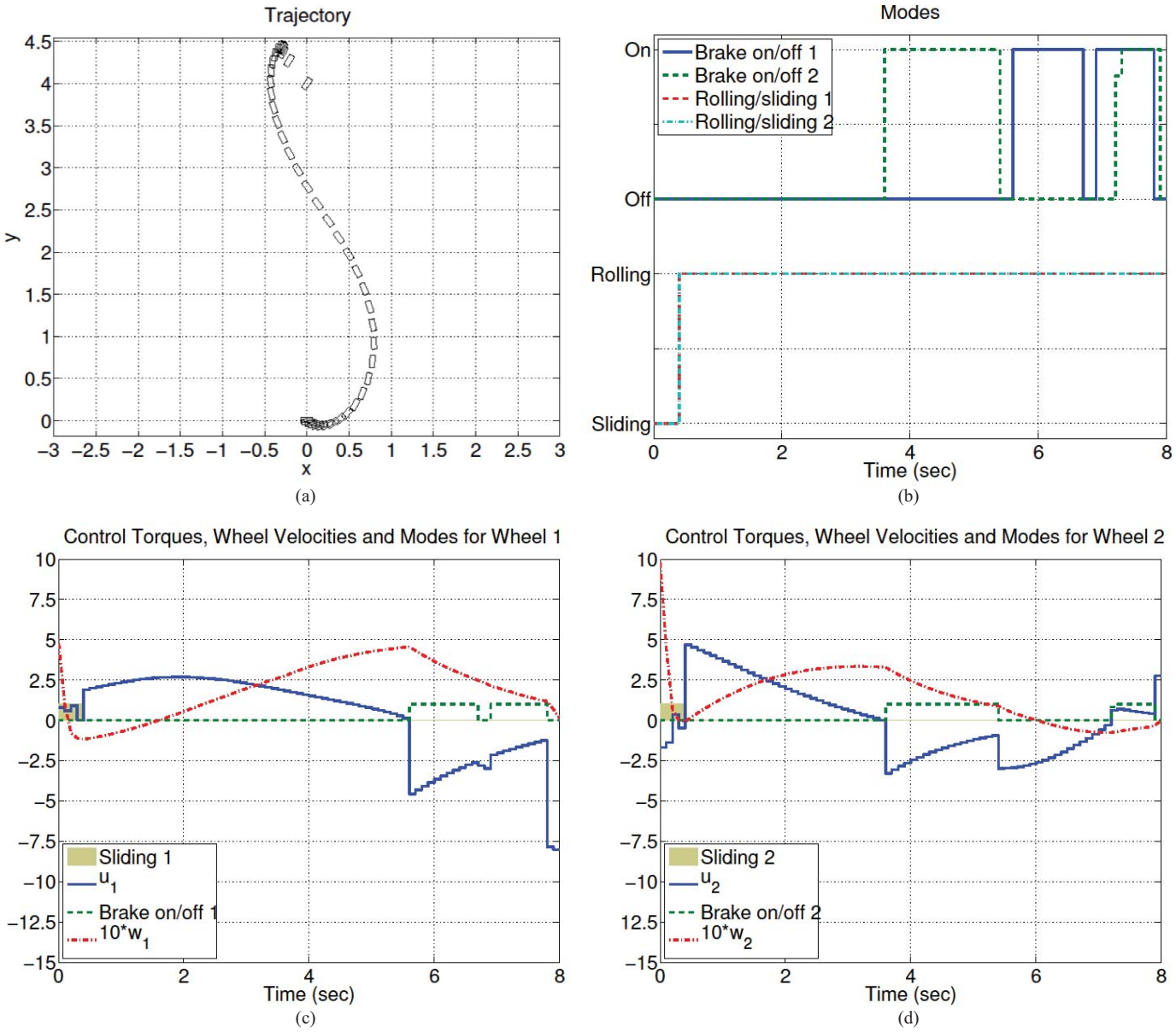

Fig. 2. Nominal behavior of the WMR for stabilization to a point (case 1). (a) Trajectory of the WMR (case 1). (b) Switching behavior of the WMR (case 1). (c) and (d) Control torques, wheel velocities, and modes for wheel 1 (c) and wheel 2 (d); (case 1).

its distance to the origin is slightly less than 2.8m, due, for example, to a camera which scans the immediate environment. However, it incorrectly estimates that in the patch $\mu_s = 0.02$ (versus the real value of 0.002) and $\mu_d = 0.01$ (versus the real value of 0.0001). Case 2 tests the robustness of the HMPC controller. In addition, case 3 tests how well the controller can adapt to the changing information about the environment. Simulation results for cases 2 and 3 appear in Figs. 3 and 4, respectively.

In case 2, at 3.5s the robot starts braking prior to encountering the slippery patch. Up to this point, the behavior of the robot is identical to the nominal behavior shown in Fig. 2. At about 3.7s, the WMR hits the slippery patch and both wheels (autonomously) switch from rolling to sliding. In Fig. 3(c) and (d), the event of the robot entering and exiting the slippery patch is denoted by vertical lines. While the robot is on the slippery patch, one observes from Fig. 3(c) and (d) that the brake remains off for wheel 1 while wheel 2 pumps (turns on and off repeatedly) the brake in an effort to reduce sliding since the PI penalizes sliding. The pumping action of wheel 2, combined with the rolling of wheel 1, also starts a slight reorientation of the WMR back toward the origin. After leaving the slippery patch at about 4.3s, the increased value of the coefficient of friction μ_d eventually leads to the relative velocity between the wheels and the ground becoming zero, resulting in rolling. At this point, corrective action of the HMPC controller begins a gradual turning and stopping process resulting in stabilization of the WMR to the origin with zero final velocity. This process of turning and slowing is accomplished by coordinated braking between the wheels as

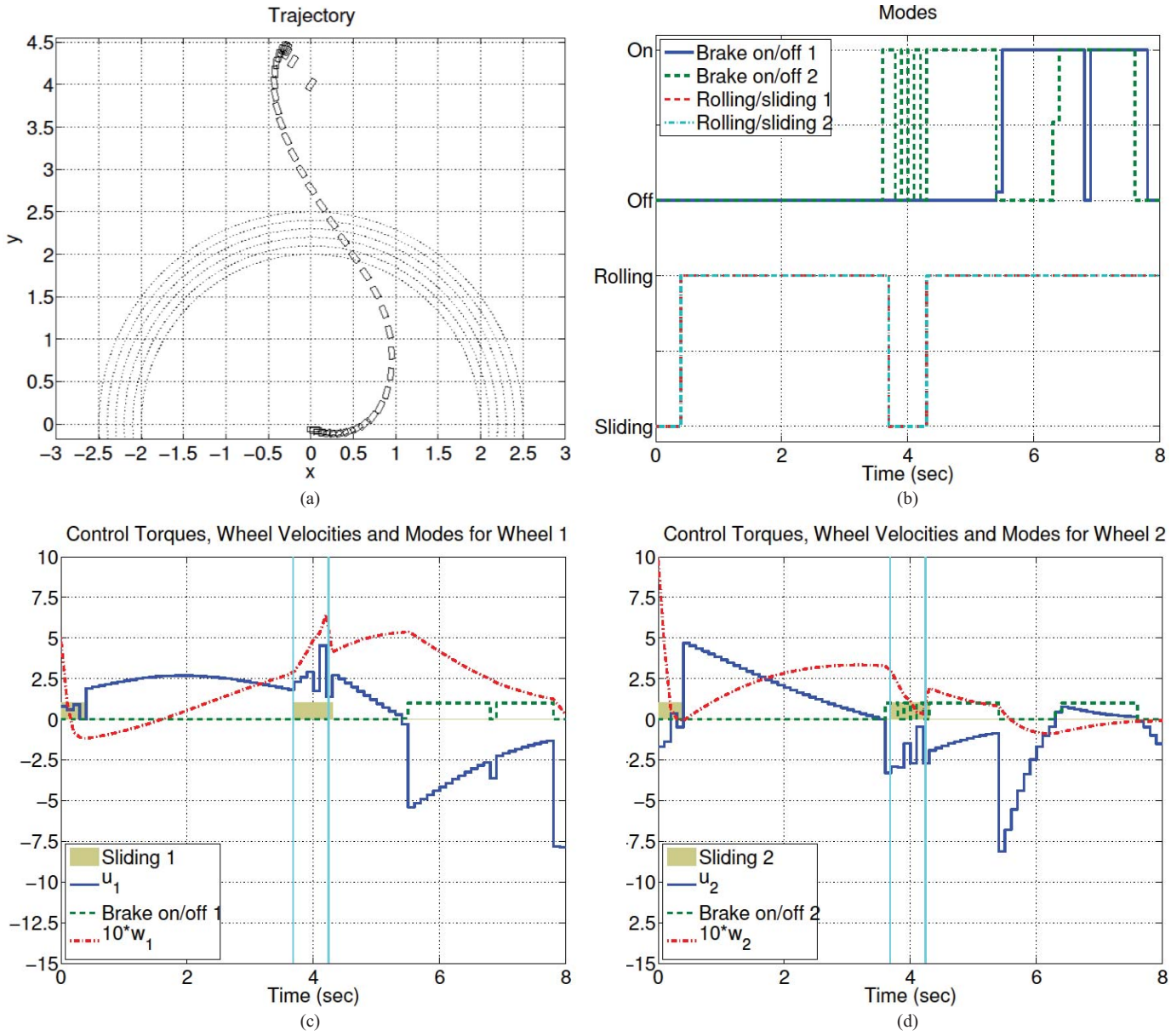

Fig. 3. Response of the WMR to an unexpected slippery patch (case 2). (a) Trajectory of the WMR (case 2). (b) Switching behavior of the WMR (case 2). (c) and (d) Control torques, wheel velocities, and modes for wheel 1 (c) and wheel 2 (d); (case 3).

well as the application of negative propelling torques, similar to the nominal case in Fig. 2.

Case 3 is similar to case 2, with the main difference being a sensor that detects the presence of an ice patch before the WMR enters it. Vertical lines in Fig. 4(c) and (d) denote the instances when the WMR detects, enters, and exists the ice patch, respectively. When the ice patch is detected at 3.4s, the WMR applies a large negative torque to both wheels in an attempt to slow down. A larger negative torque on wheel 2 than on wheel 1 also produces a slight turning action; as a result the WMR enters the slippery patch almost perpendicularly. Note that regenerative braking could not produce such large torques because it depends on wheel speed. Just before entering the slippery patch at 3.7s, the robot reduces the torques in order to prevent slippage. However, as the robot enters the patch and encounters the coefficient of friction that is smaller than anticipated, it reacts by increasing the torques and trying to turn and stay on the desired course. At about 3.9s, the WMR begins to slide, so the controller reacts by reducing the torques. Note that the robot enters the patch later than in case 1 because the controller anticipates the ice patch. Subsequently, the controller action brings both wheels back to rolling. The robot then engages the regenerative brake on wheel 2 at 4.4s in order to steer. However, due to the erroneous information about the coefficients of friction, it slides again at approximately 4.5s. The coordinated action of the controller keeps the brake on wheel 2 engaged while at the same time propelling wheel 1 to bring its relative velocity to 0. The WMR exits the slippery patch at approximately 5.2s but it continues to slide. However, a large coefficient of friction brings wheel 1

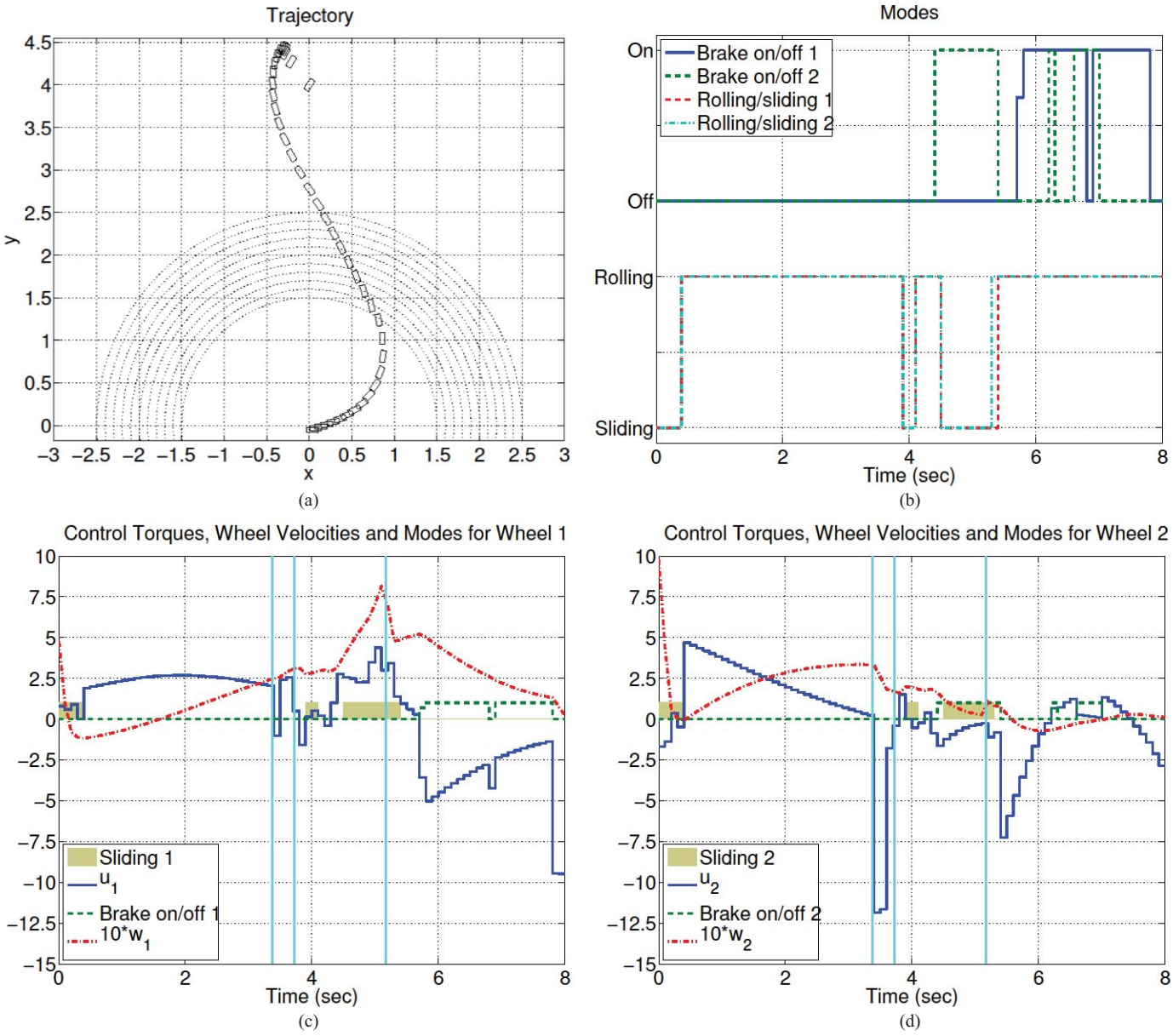

Fig. 4. Response of the WMR to a slippery patch with advance notice (case 3). (a) Trajectory of the WMR (case 3). (b) Switching behavior of the WMR (case 3). (c) and (d) Control torques, wheel velocities, and modes for wheel 1 (c) and wheel 2 (d); (case 3).

to rolling at 5.3s, and wheel 2 to rolling at 5.4s. After this point, the robot uses a similar coordination between braking and active propelling as in cases 1 and 2 to slow down and arrive at the origin with zero velocity, as desired.

In both cases 2 and 3, the WMR reaches the target in the required time. From the figures we can see that despite the disturbances, the HMPC controller makes the WMR perform as desired: the WMR is successfully stabilized to the predefined set within an allotted time in spite of the initial sliding condition and external disturbances. We thus conclude that the proposed approach provides a numerically efficient solution to a complex nonlinear control problem that achieves excellent robustness and performance.

VI. Conclusion

This paper presented the application of hybrid MPC to the stabilization of WMRs equipped with regenerative brakes and subject to wheel slippage. The approach is based on theoretical insights provided in [1] and [2] using numerical techniques suggested in [22] and [23]. Regenerative braking and wheel slippage in the WMR result in a hybrid system with controlled and autonomous switches [27]. Stabilization of the WMR to a desired configuration is formulated as a hybrid MPC problem. Using the results from [1] and [2], the hybrid MPC problem can be formulated as a smooth optimization problem. It can thus be effectively solved numerically using collocation and the quadratic penalty function approach. Simulation results show physically meaningful and robust performance.

Although the WMR studied in this paper is a simple two-wheeled mobile robot, the approach can be easily extended to other WMRs or other complex robotic systems. In particular, the system considered in this paper can be seen as an abstraction of a hybrid electric vehicle with an active safety control system [28], [29]. The results of this paper

thus have implications for safe control of vehicles subject to slippage.

REFERENCES

[1] S. Wei, K. Uthaichana, M. Žefran, R. DeCarlo, and S. Bengea, "Applications of numerical optimal control to nonlinear hybrid systems," *Nonlin. Anal., Hybrid Syst.*, vol. 1, no. 2, pp. 264–279, 2007.

[2] S. C. Bengea and R. A. DeCarlo, "Optimal control of switching systems," *Automatica*, vol. 41, no. 1, pp. 11–27, 2005.

[3] A. DeLuca, G. Oriolo, and C. Samson, "Feedback control of a nonholonomic car-like robot," *Robot Motion Plann. Control, Lect. Notes Control Inform. Sci.*, vol. 229, pp. 171–253, May 1998.

[4] S. Pekarak, K.Uthaichana, S. Bengea, R. DeCarlo, and M. Žefran, "Modeling of an electric drive for a HEV supervisory level power flow control problem," in *Proc. IEEE Conf. Veh. Power Propuls.*, 2005, pp. 396–401.

[5] K. Uthaichana, R. DeCarlo, S. Bengea, S. Pekarek, and M. Žefran, "Hybrid model predictive control tracking of a sawtooth driving profile for an HEV," in *Proc. Amer. Control Conf.*, 2008, pp. 967–974.

[6] S. Richter and R. DeCarlo, "Continuation methods: Theory and applications," *IEEE Trans. Joint Spec. Issue Large Scale Syst. AC/CAS/SMC*, vol. 28, no. 6, pp. 347–352, Mar. 1983.

[7] H. Wacker, *Continuation Methods*. New York: Academic Press, 1978.

[8] C. Canudas de Wit and R. Roskam, "Path following of a 2-dof wheeled mobile robot under path and input torque constraints," in *Proc. IEEE Int. Conf. Robot. Autom.*, Aug. 1991, pp. 1142–1147.

[9] B. d'Andrea Novel, G. Bastin, and G. Campion, "Modelling and control of non holonomic wheeled mobile robots," in *Proc. IEEE Int. Conf. Robot. Autom.*, Apr. 1991, pp. 1130–1135.

[10] C. Samson and K. Ait-Abderrahim, "Feedback control of a nonholonomic wheeled cart in cartesian space," in *Proc. IEEE Int. Conf. Robot. Autom.*, Apr. 1991, pp. 1136–1141.

[11] G. Campion, B. d'Andrea Novel, and G. Bastin, "Modelling and state feedback control of nonholonomic mechanical systems," in *Proc. IEEE Conf. Decision Control*, Apr. 1991, pp. 1184–1189.

[12] N. Sarkar, X. Yun, and V. Kumar, "Control of mechanical systems with rolling constraints application to dynamic control of mobile robots," *Int. J. Robot. Res.*, vol. 13, no. 1, pp. 55–69, 1994.

[13] D. Gu and H. Hu, "Model predictive control for simultaneous robot tracking and regulation," in *Proc. Int. Conf. Intell. Mechatron. Autom.*, 2004, pp. 212–217.

[14] D. Wang and G. Xu, "Full-state tracking and internal dynamics of nonholonomic wheeled mobile robots," *IEEE/ASME Trans. Mechatron.*, vol. 8, no. 2, pp. 203–214, Feb. 2003.

[15] R. Balakrishna and A. Ghosal, "Modeling of slip for wheeled mobile robots," *IEEE Trans. Robot. Autom.*, vol. 11, no. 1, pp. 126–132, Jan. 1995.

[16] W. Leroquais and B. A. Novel, "Modeling and control of wheeled mobile robots not satisfying ideal velocity constraints: The unicycle case," in *Proc. IEEE Conf. Dec. Control*, Mar. 1996, pp. 1437–1442.

[17] M. Zefran and J. W. Burdick, "Design of switching controllers for systems with changing dynamics," in *Proc. IEEE Conf. Dec. Control*, Dec. 1998, pp. 2113–2118.

[18] M. S. Branicky, V. S. Borkar, and S. K. Mitter, "A unified framework for hybrid control: Model and optimal control theory," *IEEE Trans. Autom. Control*, vol. 43, no. 1, pp. 31–45, Jan. 1998.

[19] A. F. Filippov, *Differential Equations with Discontinuous Righthand Sides*. Dordrecht, The Netherlands, Kluwer Acad., 1988.

[20] V. I. Utkin, *Sliding Modes in Control and Optimization*. Berlin, Germany: Springer-Verlag, 1992.

[21] P. T. Boggs and J. W. Tolle, "Sequential quadratic programming," *Actanumerica*, vol. 4, pp. 1–51, Nov. 1995.

[22] P. E. Gill, W. Murray, and M. A. Saunders, "SNOPT: An SQP algorithm for large-scale constrained optimization," *SIAM Rev.*, vol 47, no. 1, pp. 99–131, 2005.

[23] D. P. Bertsekas, *Constrained Optimization and Lagrange Multiplier Methods*. San Francisco, CA: Academic Press, 1982.

[24] E. F. Camacho and C. Bordons, *Model Predictive Control*. Berlin, Germany: Springer-Verlag, 2004.

[25] A. Bemporad and M. Morari, "Control of systems integrating logic, dynamics, and constraints," *Automatica*, vol. 35, no. 3, pp. 407–427, 1999.

[26] O. V. Stryk, "Numerical solution of optimal control problems by direct collocation," *Opt. Control Int. Series Numer. Math.*, vol. 111, pp. 129–143, Mar. 1993.

[27] A. J. van der Schaft, J. M. Schumacher, *An Introduction to Hybrid Dynamical Systems*. Berlin, Germany: Springer-Verlag, 1999.

[28] A. Trachtler, "Integrated vehicle dynamics control using active brake, steering and suspension systems," *Int. J. Veh. Des.*, vol. 36, no. 1, pp. 1–12, 2004.

[29] P. Falcone, H. E. Tseng, F. Borrelli, J. Asgari, and D. Hrovat, "MPC-based yaw and lateral stabilisation via active front steering and braking," *Veh. Syst. Dynam., Int. J. Veh. Mechan. Mobil.*, vol. 46, no. 1, pp. 611–628, 2008.

[30] S. Wei, M. Žefran, K. Uthaichana, and R. A. DeCarlo, "Hybrid model predictive control for stabilization of wheeled mobile robots subject to wheel slippage," in *Proc. IEEE Int. Conf. Robot. Autom.*, Apr. 2007, pp. 2373–2378.

[31] R. Meyer, R. DeCarlo, P. Meckl, C. Doktorcik, and S. Pekarek, "Hybrid model predictive power flow control of a fuel cell-battery vehicle," in *Proc. Amer. Control Conf.*, 2011, pp. 2725–2731.

[32] M. Oettmeier, J. Neely, S. Pekarek, R. DeCarlo, and S. Uthaichana, "MPC of switching in a boost converter using a hybrid state model with a sliding mode observer," *IEEE Trans. Ind. Electron.*, vol. 56, no. 9, pp. 3453–3466, Sep. 2009.

[33] *New York State Department of Motor Vehicles*. "Driver's Manual," (2011) [Online]. Available: http://www.dmv.ny.gov/broch/MV21.pdf

[34] S. V. Emelyanov, *Variable Structure Control Systems*. Berlin, Germany: Springer-Verlag, 1967.

[35] J. Lygeros, K. H. Johansson, S. N. Simic, J. Zhang, and S. S. Sastry, "Dynamical properties of hybrid automata," *IEEE Trans. Autom. Control*, vol. 48, no. 1, pp. 2–17, Jan. 2003.

[36] D. T. Greenwood, *Principles of Dynamics*. Englewood Cliffs, NJ: Prentice-Hall, 1988.

[37] M. D. Bernardo, C. J. Budd, A. R. Champneys, and P. Kowalczyk, *Piecewise-Smooth Dynamical Systems: Theory and Applications*. Berlin, Germany: Springer-Verlag, 2008.

[38] K. Deimling, *Multivalued Differential Equations*. Berlin, Germany: Walter de Gruyter, 1992.

Shangming Wei received the B.S. and M.S. degrees from Shanghai Jiao Tong University, Shanghai, China, in 1995 and 1998, respectively, and the Ph.D. degree from the University of Illinois at Chicago, Chicago, in 2007, all in electrical engineering. His doctoral research focused on control of hybrid robotic systems.

He is currently with MathWorks, Inc., Natick, MA. He was with CNH America LLC, Burr Ridge, IL, from 2008 to 2012, where he was involved in vehicle modeling and hardware-in-the-loop simulation.

Kasemsak Uthaichana (M'03) received the B.S. degree in electrical, computer, and systems engineering from Rensselaer Polytechnic Institute, Troy, NY, in 2000, and the M.S. and Ph.D. degrees in electrical and computer engineering from Purdue University, West Lafayette, IN, in 2002 and 2006, respectively. His doctoral research focused on modeling and power flow control for parallel hybrid electric vehicles.

He is currently with the Department of Electrical Engineering, Chiang Mai University, Chiang Mai, Thailand, where he is an Assistant Director with Science and Technology Park. He was with Caterpillar Inc., Peoria, IL, from 2007 to 2008, where he was involved in integrated power systems control software. His current research interests include power management in hybrid vehicles, proton-exchange membrane fuel cells, Li-ion batteries, automated TIG welding robot, and system estimation and compensation.

Dr. Uthaichana is a member of the IEEE Control Systems Society and the IEEE Power and Energy Society.

Miloš Žefran received the B.S. and M.S. degrees in electrical engineering and mathematics from the University of Ljubljana, Ljubljana, Slovenia, and the M.S. degree in mechanical engineering and the Ph.D. degree in computer science from the University of Pennsylvania, Philadelphia, in 1995 and 1996, respectively.

Since 1999, he has been with the Department of Electrical and Computer Engineering, University of Illinois at Chicago, Chicago, where he is currently an Associate Professor. He was an NSF Postdoctoral Scholar with the California Institute of Technology, Pasadena, from 1997 to 1999, after which he joined the Rensselaer Polytechnic Institute, Troy, NY. His current research interests include haptics, robot networks, and cyber-physical systems.

Dr. Žefran was a recipient of the NSF Career Award in 2000. He is an Associate Editor of the IEEE TRANSACTIONS ON CONTROL SYSTEMS TECHNOLOGY and the IEEE TRANSACTIONS ON AUTOMATION SCIENCE AND ENGINEERING.

Raymond DeCarlo was born in Philadelphia, PA. He received the B.S. and M.S. degrees in electrical engineering from the University of Notre Dame, Notre Dame, IN, in 1972 and 1974, respectively, and the Ph.D. degree under the supervision of Dr. R. Saeks from Texas Tech University, Lubbock, in 1976.

He joined Purdue University, West Lafayette, IN, in 1977, as an Assistant Professor of electrical engineering, becoming an Associate Professor and a Full Professor in 1982 and 2005, respectively. He was with the General Motors Research Labs during the summers of 1985 and 1986.

Dr. DeCarlo was an Associate Editor of *Technical Notes and Correspondence*, and *Survey and Tutorial Papers* and the IEEE TRANSACTIONS ON AUTOMATIC CONTROL. He was the Secretary-Administrator of the IEEE Control Systems Society, a member of the Board of Governors from 1986 to 1992 and from 1999 to 2003, the Program Chairman for the 1990 IEEE CDC (Honolulu), and the General Chairman of the 1993 IEEE CDC (San Antonio). He was the VP for Financial Activities for the IEEE CSS in 2001 and 2002.